SANDIA REPORT

SAND2011-9415
Unlimited Release
Printed December 2011

Recommendations on the Prediction of Thermal Hazard Distances from Large Liquefied Natural Gas Pool Fires on Water for Solid Flame Models

Anay Luketa

Prepared by
Sandia National Laboratories
Albuquerque, New Mexico 87185 and Livermore, California 94550

Sandia National Laboratories is a multi-program laboratory managed and operated by Sandia Corporation, a wholly owned subsidiary of Lockheed Martin Corporation, for the U.S. Department of Energy's National Nuclear Security Administration under contract DE-AC04-94AL85000

Issued by Sandia National Laboratories, operated for the United States Department of Energy by Sandia Corporation.

Available to DOE and DOE contractors from
U.S. Department of Energy
Office of Scientific and Technical Information
P.O. Box 62
Oak Ridge, TN 37831

Telephone: (865)576-8401
Facsimile: (865)576-5728
E-Mail: reports@adonis.osti.gov
Online ordering: http://www.osti.gov/bridge

Available to the public from
U.S. Department of Commerce
National Technical Information Service
5285 Port Royal Rd
Springfield, VA 22161

Telephone: (800)553-6847
Facsimile: (703)605-6900
E-Mail: orders@ntis.fedworld.gov
Online order: http://www.ntis.gov/help/ordermethods.asp?loc=7-4-0#online

SAND2011-9415
Unlimited Release
Printed December 2011

Recommendations on the Prediction of Thermal Hazard Distance from Large Liquefied Natural Gas Pool Fires on Water for Solid Flame Models

Anay Luketa
Fire and Aerosol Sciences Department

Sandia National Laboratories
P.O. Box 5800
Albuquerque, New Mexico

ABSTRACT

The objective of this work is to provide recommendations on predicting thermal hazard distances resulting from large liquefied natural gas (LNG) pool fires on water. The recommendations pertain to an integral model approach and its pertinent parameters such as burn rate, flame height, surface emissive power (SEP), and transmissivity. These recommendations are based upon knowledge gained from conducting experiments of LNG pool fires on water at Sandia National Laboratories in New Mexico in 2009 in addition to earlier, smaller scale tests. The 83 diameter meter test resulted in a 56 m diameter pool fire which is the largest LNG pool fire test performed on water or land to date.

ACKNOWLEDGEMENTS

The author would like to thank the following individuals for their review of the manuscript: S. Tieszen, T. Blanchat, and M. Hightower.

CONTENTS

LIST OF FIGURES

LIST OF TABLES

1 EXECUTIVE SUMMARY

The objective of this work is to provide recommendations on predicting thermal hazard distances resulting from large liquefied natural gas (LNG) pool fires on water using solid flame models. These recommendations are based upon knowledge gained from conducting experiments of LNG pool fires on water. The interest in LNG pool fires is motivated by the concern over potential hazards arising from a spill event associated with the ships transporting the LNG (Hightower 2004, Luketa 2008). The Government Accountability Office (GAO), in report GAO-07-316, recommended that the Secretary of Energy ensure the Department of Energy (DOE) incorporate key issues identified in their report into DOE's current LNG study, including large scale LNG fire testing. DOE tasked Sandia National Laboratories (SNL) to perform a set of experiments to improve the understanding of the physics and hazards of large LNG spills on water with concurrent fires. These are the largest LNG pool fire tests performed on water or land to date. The description and results of these tests are provided in a Sandia report, "The Phoenix Series Large Scale LNG Pool Fire Experiments" (Blanchat, et al. 2011). The parameters used in the 2004 and 2008 Sandia LNG reports (Hightower 2004, Luketa 2008) were based on then available data of much smaller scale (Raj 1979). In keeping with the principal of using the best available data, the parameters have been adjusted to reflect the newly acquired data. The updated parameter values provided in Table 1 are considered conservative and result in approximately 2% and 7-8% lower thermal hazard distances than provided in the 2004 and 2008 Sandia reports, respectively. It must be emphasized as in the 2004 and 2008 Sandia reports that hazard distances will change depending on the surroundings conditions and the scenarios associated with the site. Thus, site-specific analyses should be performed.

Table 1: Recommended parameter values for solid flame model.

Parameter	***Recommended nominal value***
Burn rate (m/s)	3.5×10^{-4} $(2.6 – 4.5 \times 10^{-4})$*
flame height (m)	SNL correlation, Eq. (1) (eqns. 1a, 1b)*
SEP (kW/m^2)	286 (248 – 326)*
Transmissivity	Wayne formula, Eq. (3) (±10%)*

*range of uncertainty

Discussion is provided on phenomena observed during the large-scale Sandia LNG pool-fire tests on water not previously indentified from other smaller LNG pool fire tests on water (Raj 1979). These include water entrainment, flame stability, and hydrate formation. The SNL LNG

pool fire tests and other studies suggest that entrained water has the potential to reduce soot production and enhance soot oxidation, thereby reducing smoke production. This is a plausible explanation for the lack of smoke shielding witnessed during the 83-m diameter test that resulted in a 56-m diameter pool fire conducted at Sandia (Blanchat, et al. 2011). During the Sandia testing it was also observed that the flame has a tendency to not have sustained burning in the upwind edge of the pool. Since it is very difficult to predict the extent of non-burning regions across the pool it is recommended for safety purposes to assume the pool area is fully burning. Hydrate formation also has a potential to form but will not be stable in locations with water temperatures above freezing, especially in marine environments that have agitation and higher saline contents. For safety purposes it is conservative to assume no hydrate formation.

2 INTRODUCTION

The objective of this work is to provide recommendations on predicting thermal hazard distances resulting from large liquefied natural gas (LNG) pool fires on water using solid flame models. The interest in LNG pool fires is motivated by the concern over potential hazards arising from a spill event associated with the ships transporting the LNG (Hightower 2004, Luketa 2008). In such an event, a large pool fire on the order of 100s of meters is considered possible. Thus, it is important to predict thermal hazard distances in order to protect the public and to reduce or prevent fire propagation to nearby structures.

The approach to modeling LNG pool fires range from the very simple, such as a point source representation, to the very complex, such as using computational fluid dynamics (CFD) for turbulent reacting flow. The recommendations in this report pertain to a simplified modeling approach using a solid flame model and its pertinent parameters such as burn rate, flame height, surface emissive power (SEP), and transmissivity. These recommendations are based upon knowledge gained from conducting experiments of LNG pool fires on water at Sandia in addition to earlier smaller scale studies. The Government Accountability Office (GAO), in report GAO-07-316, recommended that the Secretary of Energy ensure the Department of Energy (DOE) incorporate key issues identified in their report into DOE's current LNG study, including large scale LNG fire testing. DOE tasked Sandia National Laboratories (SNL) to perform a set of experiments to improve the understanding of the physics and hazards of large LNG spills on water with concurrent fires. The new data are the largest LNG pool fire tests performed on water or land to date. The results are provided in a Sandia report, "The Phoenix Series Large Scale LNG Pool Fire Experiments". (Blanchat, et al. 2011).

Integral or solid flame models represent the surface of the flame with a simple, usually cylindrical, geometry as shown in Figure 1 (Mudan 1984). The heat flux as a function of distance is determined from the equation, $\dot{q}'' = EF\tau$. The thermal radiation, E, is uniformly emitted from this surface and is the average surface emissive power (SEP). For an assumed geometry, the geometric view factor, F, which is the fraction of radiant energy that is received by an object's field of view, can be determined exactly. The transmissivity,τ, ranging from values of 0 to 1 is the degree of atmospheric attenuation due principally to H_2O and CO_2. In order to capture the tilting of the flame due to wind, a tilted cylindrical flame shape is typically used (Mudan 1987). Flame length, tilt and drag necessary to determine flame shape and view factors are based upon empirical correlations. For pool fires with simple pool geometries, and where parameters are well known, these models provide good agreement with experiment.

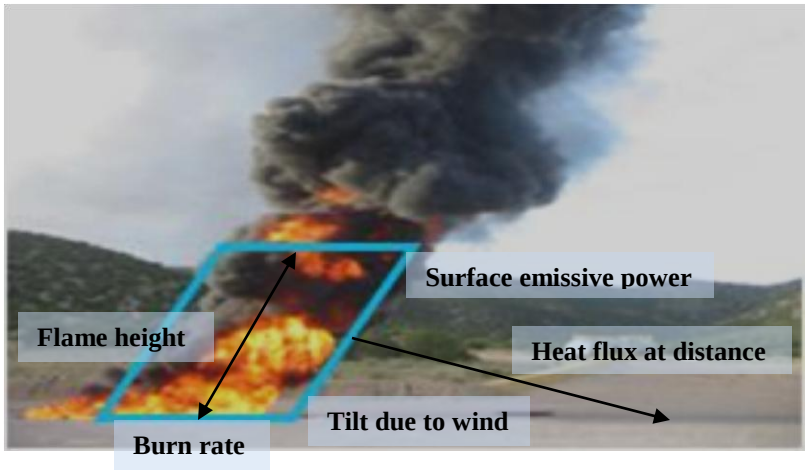

Figure 1: Tilted cylinder representation using solid flame model

Solid flame models are appropriate for sites which are not in close proximity to urban locations. However, for sites near populations where there are nearby structures that can alter the nature of the pool fire, such as in pool geometry or through fire propagation to other structures, these models do not have the capability to predict the hazards for these cases. In contrast to an open ocean, the numerous structures comprising an urban environment will affect the distribution of energy or heat received to populations and structures by either providing shielding, thereby reducing the amount received, or creating 'hot spots' from recirculation zones or reflecting surfaces, thereby increasing the amount received. Additionally, the presence of obstacles can affect thermal hazards by providing additional fuel for fire propagation.

To make hazard assessments in more complex environments, computational fluid dynamics (CFD) models should be considered. CFD based models have the ability to model irregular geometries as well as fire and smoke propagation. It should be noted that thermal damage is one aspect of assessing the hazards arising from a LNG pool fire in an urban environment. Smoke propagation would also have to be included in analyses since it too can be a hazard such as when drafted in through ventilation systems of buildings. Human behavior during evacuations should also be considered since it affects the number of casualties/injuries and hence total damage. With large populations and complicated pathways for exit, effective evacuation efforts can be extremely difficult. All of these factors should be considered to understand the damage potential from an LNG pool fire in an urban environment.

The following provides a description of the behavior of LNG pool fires compared to most other hydrocarbons, specifically with regards to soot production, flame height, and burn rate. Also discussed are wind effects and water conditions in consideration of observations during the SNL tests. The previous recommendations for parameters used in the thermal hazard calculation in the 2004 and 2008 Sandia LNG reports (Hightower 2004, Luketa 2008) are also discussed and compared to recommendations in this work.

3 BEHAVIOR OF LNG POOL FIRES

3.1 Soot production

LNG is a cryogen and is comprised mostly of methane and smaller amounts of ethane and propane, as well as other heavier hydrocarbons. LNG pool fires are very different in behavior than most other hydrocarbon pool fires at similar scale, specifically in smoke formation, burn rate, and flame height, all of which effect thermal hazard distances. Smoke is made up of a mixture of gases, vapors, and particulate matter from a fire. Carbon particulates, or soot, is included as a particulate matter of smoke and is responsible for the luminosity of the fire, as well as, the black clouds often seen around fires. A sufficient layer of black smoke will absorb a significant portion of the radiation resulting in a much lower emission to the surroundings and hence reduce thermal hazard distances. Smoke is a result of incomplete combustion which is affected by radiative losses and limited oxygen supply.

At similar diameters LNG pool fires form significantly less smoke than other hydrocarbons as shown in Figure 2. The 10 m diameter LNG pool fire is optically thin, that is, the local volume of flames is not able to absorb the local emitted radiation before it leaves the flame envelope and hence the flame appears transparent, whereas the 7.9 m JP-8 pool fire is optically thick and has a significant smoke layer covering the flame envelope.

Pool fires will be optically thin up to a certain diameter and then transition to becoming optically thick where the flame is no longer transparent and the local soot production becomes saturated to the point that local radiation emission is absorbed within the flame envelope. The radiation emitted on the outer surface of the flame envelope originates at a layer near the surface. The surface emissive power (SEP) which is the energy emitted per unit time per unit area is then a function of the surface area of the flame and not the volume as for optically thin fires. As the scale of the fire increases the rate of soot production overcomes the rate of soot oxidation and smoke begins to form and eventually a diameter is reached in which so much smoke is formed that it nearly covers the entire flame except for a region near the pool surface where a continuous luminous zone persists. In this instance, the SEP includes the effect of smoke on the thermal radiation emitted to an object at a distance from the fire. Thus, with increasing pool diameter the average SEP over the flame will first increase with increasing fire diameter due to reaching the optically thick limit then decrease with further increases in fire diameter due to the increasing smoke layer coverage. LNG pool fire experiments conducted at Sandia have exhibited a trend of increasing smoke production with increasing diameter as seen in Figure 3. However, the relative smoke coverage even at a diameter of 56 m is still much less than a JP-8 fire at 7.9 m.

(a) **(b)**

Figure 2: a) 10-m diameter LNG pool fire and, b) 7.9-m diameter JP-8 pool fire both performed at SNL (Albuquerque, NM).

(a) **(b)** **(c)**

Figure 3: LNG pool fires of diameters a) 10-m, b) 21-m, and c) 56-m conducted at Sandia.

One of the most interesting aspects observed from the 83-m diameter LNG experiment that resulted in a 56-m diameter pool fire is the less smoke production than the 35 m diameter LNG pool fire Montoir experiments conducted on land as shown in Figure 4 (Nedelka 1989, Tucker 1988, British Gas 1988). While smoke was produced in the SNL test it mostly formed in small amounts at lower elevations and rolled up to accumulate near the tip then exited the flame. Thus, no significant smoke shielding was observed in the SNL tests while it was quite evident in the upper half of the flame in the Montoir tests. This is contrary to the trend that smoke production should increase with larger diameters. The two main differences between the Montoir and SNL tests are elevation and water. There is also the difference of fuel composition. The Montoir tests used LNG mixed with heavier hydrocarbons while the SNL tests used fairly pure LNG (>99% methane). The fuel composition difference is not considered to be a factor because gas composition measurements in the Montoir tests indicate that for the duration of measurements there was at least 99-mol% methane boiling from the pool. Thus, measurements from a methane fire were obtained, similar to the SNL tests.

Figure 4: Montoir 35 m LNG pool fire on land (left) and SNL 56 m LNG pool fire on water (right).

Due to the elevation of Albuquerque, N.M. the SNL tests were conducted in an ambient pressure 17% lower than that of sea level while the Montoir tests were conducted at sea level. The extent that atmospheric pressure affects soot production for optically-thick turbulent pool fires has yet to be substantiated in the fire science community. Existing theoretical approaches do not account for the difference shown in Figure 4.

One approach to predict the influence of pressure is pressure scaling modeling which is based upon dimensionless arguments. The idea behind pressure scaling is to gain understanding about larger fires from smaller scale tests which has the obvious advantage of lower cost and increased safety. The scaling involves altering the pressure in which a test performed under elevated pressure is equivalent to a larger test performed under a lower pressure. Thus, the SNL test at lower pressure is equivalent to performing a smaller scale test at a higher pressure such as that of sea-level. Pressure scaling is effective for pool diameters under around 1 m and for certain physical quantities such as fuel regression rate and upward flame spread (Quintiere 1989), but for larger optically-thick fires where radiation becomes dominant over convective heat transfer both convection/diffusion and radiation scaling cannot be satisfied (Corlett 2008). For any scaling relation there must be validation by comparing to pool fires that are in the fully turbulent regime since heat and mass transfer characteristics are very different than laminar flames. Thus, the scaling rule should be able to predict information about 'large-scale' turbulent fires from information obtained at 'small-scale' performed under elevated pressure. This has not been achieved for the prediction of soot production and oxidation using pressure scaling modeling.

Even for laminar flames, pressure scaling dependence has shown not to be independent of fuel type and similar throughout a flame regarding soot volume fraction. Pressure scaling experiments on 4.4 mm diameter laminar methane diffusion flames up to 2.5MPa found that local peak values of soot volume fraction scales with pressure as $p^{1.2}$, while path-integrated soot volume fraction values have a different trend with no pressure dependence at 65% of the flame height, and a $p^{0.6}$ scaling at 85% of the flame height (McCrain 2005). Ethylene indicated a

different dependence of $p^{1.7}$ for local peak values, and $p^{1.2}$ for path-integrated values at 65% flame height and $p^{1.2}$ at 85% flame height. This indicates that pressure dependent scaling may not be the correct scaling parameter for soot production due to the different power dependencies at various locations of the flame. Thus, there is reason to believe that pressure may not have a significant effect on surface emissive power. Further evidence is provided by the similar surface emissive power values measured using narrow and wide-angle radiometers from 10 m diameter LNG pool fire tests on water conducted at Sandia to those conducted at China Lake at sea level (Raj 1979).

Note that even if the scaling found from the laminar tests for local peak values of soot volume fraction were considered valid for optically-thick turbulent pool fires, a $p^{1.2}$ scaling would mean that the SNL test is equivalent to a 40 m diameter fire, still larger than the Montoir, but with less smoke production. This pressure scaling dependence does not explain the difference observed between the two tests. Thus, additional effects must be responsible for the contrary trend observed in smoke production.

Beyond the difference in ambient pressure between the Montoir and SNL tests, there is also the presence of water. The Montoir tests had the LNG contained in a berm whereas for the SNL test the LNG was spilled over water. Water vapor entrainment on the oxidizer side of the flame is quite evident as observed for the 56 m diameter SNL test. Water vapor is also most likely entrained on the fuel side due to vigorous boiling at the LNG/water interface. Water addition has been used to control combustion systems such as internal combustion engine performance (Dryer 1977), gas turbine systems (Zhao 2002), and steam-assisted flares (Castineira 2006), with several studies demonstrating thermal/physical and chemical effects of water addition on flames. A few pertinent studies are detailed in the following.

Zhang, et al. obtained measurements of temperature, soot volume fraction, number density, species, and polyaromatic hydrocarbons for a methane counter-flow diffusion flame with various combinations of non-heated and preheated reactants and product diluents (C. A. Zhang 1992). One of the diluents was water vapor, added in one case to the oxidizer side and another to the fuel side. The results indicate that the addition of water vapor either on the oxidizer or fuel side reduced soot volume fraction values by a factor of about 2 with a slightly greater reduction when water vapor was added to the oxidizer side. The inlet CH_4 and O_2 concentrations, flow rates and flame temperature were maintained constant, thus the effect of water vapor addition can be attributed to a chemical rather than a thermal effect. The authors believe that the chemical effect is due to the reaction $H_2O + H \rightarrow OH\cdot + H_2$ producing the hydroxyl radical, $OH\cdot$, which lowers soot precursor concentrations and oxidizes soot. The fuel side does not have oxygen that can oxidize soot, thus $OH\cdot$ production through water addition on the fuel side is a likely cause of oxidation. It was further found that CO_2 addition has less effect on inhibiting soot formation than water vapor. To explain this they cite the work by Smyth, et al. regarding concentration measurements of the $OH\cdot$ radical in a laminar, co-flowing methane-air diffusion flame (Smyth 1990). Smyth, et al. found that the reaction $H_2O + H \rightarrow OH\cdot + H_2$ is 14 times faster than the reaction $CO_2 + H \rightarrow CO + OH\cdot$ which indicates that H_2O is much more effective than CO_2 in forming $OH\cdot$.

Atreya, et al. also experimentally and numerically studied a counter-flow methane diffusion flame (Atreya 1999). One of their objectives was to determine if water has a chemical effect, and not just a physical or thermal effect on a flame. Different levels of O_2 and water in either liquid or vapor form introduced in the oxidizer stream were tested. By varying the O_2 concentration in the oxidizer stream different levels of soot production could be produced. The results show that for a 12% O_2 oxidizer stream, water as liquid droplets has a physical suppressive effect and decreases CO_2 and increases CO production with increasing water application rate (2.12 mg/s to 13.3 mg/s). The opposite trend occurs for a 30% O_2 stream due to the higher flame temperature which allows for water to be more chemically active. A 15% O_2 stream results in CO and CO_2 either following the 12% or 30% O_2 trend depending on the application rate, thus indicating competing effects of chemical enhancement and physical dilution. Based on visual observation water also reduces soot production.

Water in vapor form indicates a different trend as a function of increasing O_2 concentration. For O_2 oxidizer stream concentration levels from 15% to 25% the CO_2 increases and CO decreases as the water vapor concentration increases (tested range of 0 to 40%). The authors attribute this different behavior to volumetric expansion effects from the evaporation of liquid droplets that can alter the flow field as well as cooling effects as compared to water vapor. Note that oxidation of CO to CO_2 is an exothermic reaction that can offset up to a certain extent the cooling effect of water. The soot production also decreases based on visual observations and the flame temperature increases with increasing water vapor concentration in the flame zone. Numerical calculations investigating how flame structure is affected by flame radiation and strain rate indicate that an increase in water vapor concentration enhances flame radiation particularly at low strain rates. The authors note that water not only suppresses a flame due to cooling and dilution, but also can result in enhanced radiative heat loss due to increased water concentration, enhanced mixing due to evaporation, and a decrease in luminous flame radiation due to a reduction in the soot concentration.

Similar results have also been found for other hydrocarbons. Rao and Bardon (Rao 1984) studied a laminar diffusion flame of 5 cm in diameter for emulsions of diesel oil, toluene and benzene with water up to a 95% mole fraction. Soot concentrations were measured by gas collection above the flame. It was found that the soot concentration decreases as the water in the fuel vapor increases for all emulsions tested. Muller-Dethlefs and Schlader (Muller-Dethlefs 1976) conducted experiments of propane and ethylene premixed flames using a Bunsen burner with steam addition. A critical air-fuel ratio at which flame luminosity is suppressed was defined by measuring the ratio of C/O, excluding the oxygen provided from the added steam. It was found that with increasing steam addition the critical C/O ratio increased. Thus, less air is required to suppress flame luminosity when water is added indicating inhibition of carbon formation. Richard, et al., (Richard 2003) conducted experiments of 10 cm diameter heptanes pool fires with water vapor addition from boiling water underneath the fuel layer. With water addition both the soot yield and CO decreased and CO_2 increased indicating the inhibition of soot formation.

These studies clearly demonstrate that water addition either on the fuel or oxidizer side has chemical and thermal effects. For optically-thin flames, where gas-band radiation dominates, the

suppression of soot will reduce the net heat flux radiated to a distant object, but for optically-thick fires in which the flame is soot saturated the effect of water vapor will be to suppress smoke formation with the consequences of increasing the net heat flux radiated to an object outside the fire. Thus, water addition is a plausible explanation for the discrepancy seen between the optically-thick SNL and Montoir tests.

3.2 Burn Rate and Flame Height

The volatilization rate, herein called the burn rate, affects thermal hazard distances by altering the size of an unconstrained pool where higher burn rates results in smaller pools and lower burn rates in larger pools. Because LNG is a cryogenic liquid, it has a higher burn rate by roughly an order of magnitude as compared to other higher molecular weight hydrocarbons. The burn rate affects flame height, H, where higher burn rates result in an increase in flame height. Time-averaged flame height is usually defined as the height at which the intermittency reaches a value of 0.5, while maximum height is defined at an intermittency level of 0.05. Intermittency is defined as the fraction of time the flame is at a certain height. The view factor is very sensitive to flame height at distances not close to the fire (> 1 pool diameter). View factors are used to determine how much radiative flux an object receives. Thus, an increase in flame height and hence view factor will result in an increase in the heat flux to an object, thereby increasing the thermal hazard distances. While an increase in burn rate will tend to reduce hazard distances by virtue of the reduction in pool diameter, the associated increase in flame height will tend to increase hazard distances. The competing effect that dominates will depend upon the diameter of the fire.

Pool shape also affects the flame height. For instance, consider the limiting conditions of a trench fire where the height is proportional to the shortest dimension. A very narrow trench fire would provide a much lower H/D than if it were circular and given equivalent areas. The difference could be an order of magnitude depending on the area and trench dimensions.

Additionally, wind can affect flame height. The flame height can be reduced from 10% to 40% depending on pool size, wind speed, and what correlation is used. The existing wind tilt correlation predictions can have wide disparity depending on the pool size and wind speed and their range of validity is applicable to much smaller pool diameters. Thus, it is difficult to quantify the effect of wind on flame height for very large pool diameters. Due to the very strong buoyancy forces induced by these large fires it is anticipated that the tilt would be significantly less than that predicted by smaller scale test data. The important aspect to note is that the effect of wind will be to reduce the flame height from that in quiescent conditions. Thus, using flame height data applicable to quiescent conditions for wind environments will provide a conservative prediction for lower heat flux levels that tend to be several diameters from the fire.

When pool fires are subject to wind they will tilt in the downward wind direction and the base dimension of the flame will extend in the downwind dimension, also termed flame drag, while the upwind and crosswind dimensions remain relatively unchanged. The affect of flame tilt and

drag is to create an elliptical pool which can result in either increasing or decreasing the thermal hazard distances in the downwind direction depending upon the degree of tilt and the distance from the fire. Burn rate is also affected by the wind speed as shown in Figure 5 for JP-8 pool fires 18.9 m and 7.9 m in diameter where increasing wind speeds result in increasing burn rates. The Montoir tests also performed tests in different wind speeds. Comparison of wind speed measurements at similar heights of 1 m can be made for two tests where average wind speeds of 2.4 m/s and 5.7 m/s resulted in average burn rates of 0.124 kg/m^2 s and 0.14 – 0.163 kg/m^2 s, respectively (British Gas 1988).

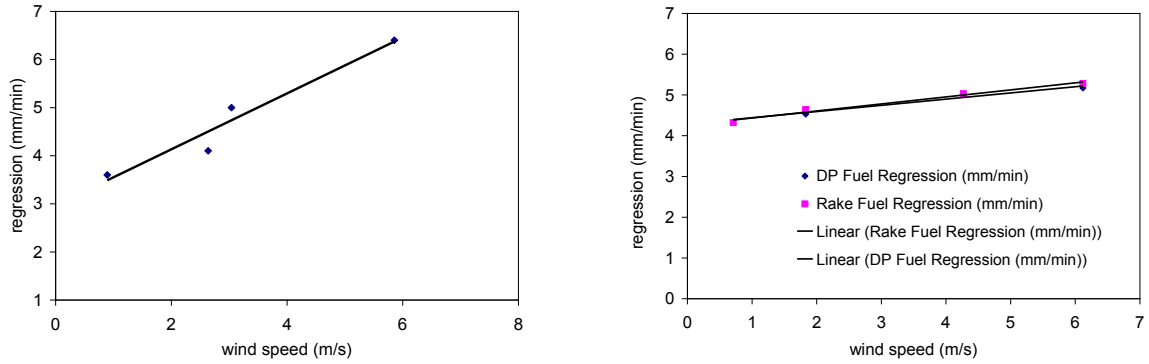

Figure 5: Regression rates as a function of wind speed for (a) 18.9 m JP-8 pool fire, 4000 gallons, China Lake (Blanchat 2002) and (b) 7.9 m JP-8 pool fire, 2200 gallons, SNL (Blanchat 2006).

3.3 Wind Effects on Flame Stability and Structure

In addition to altering flame geometry, wind also affects flame stability and structure. Observations from the SNL tests indicate that the flame did not cover the entire pool surface as shown in Figure 6 . It is instructive to discuss the nature of diffusion flames with regards to pertinent time scales in order to understand this behavior. Fuel and oxidizer are initially separate for diffusion flames and as such both must mix or diffuse

Figure 6: Occurrence of non-burning regions shown for the 10-m, 21-m, and 83- m pool (56 m fire) SNL tests.

in the same region at which chemical reaction occurs. Thus, there are chemical and diffusive

time scales to consider with regards to flame stability and extinction. The characteristic chemical reaction time, τ_c, and diffusion time, τ_d, depends on the particular flow configuration and reactants. The chemical reaction rate is typically much faster than the diffusion velocity of the gases but not for states near extinction. As the surrounding flow velocity increases the characteristic diffusion time decreases and a critical flow velocity can be reached were the chemical reaction cannot keep up with the supply of fuel and oxidant and extinction occurs. Thus, chemical reaction time limits the combustion rate in the case of extinction. When chemical times are on the order of diffusion time scales, finite rate chemistry must be considered. The Damkohler number, $Da=\tau_d/\tau_c$, is a dimensionless number used to represent the ratio of these two time scales, where a critical Da determines system-dependent flame extinction.

In conditions of wind and where the pool is not contained such that a lip does not surround the pool there is a high probably for a critical Da number to be reached. In this instance the fuel does not burn at the upwind edge of the pool surface. The extent of the non-burning region will increase with increasing wind speeds. Even without wind the entrainment induced by the fire can potentially create critical Da number regions where burning does not occur. In the case where there is a pool lip by virtue of containment, the presence of such an obstacle provides regions of reduced velocities as in the leeward side of a bluff body. This locally reduces the flow velocity thereby allowing for the chemical reaction to keep pace with the supply of reactants in these regions. It is well envisioned that since wind conditions are prevalent in scenario environments there will be a mixture of non-burning and burning pool regions due to flow-induced extinction with the fire principally anchored to the LNG ship. It is difficult to predict the partition of these regions since it depends upon the wind and spill conditions. The scenario affording the most potential regarding fire size would be a spill on the downwind side of a ship.

Wind can also affect both the dynamics of the fire plume and the level of smoke shielding. In wind conditions, the structure of the plume can change by the creation of fire whirls which can occur in pool fires such as burning of a crude oil spill on water (Soma 1991). The structure of fire whirls consists of an upward convective current generated by the fire and a swirling motion (vortex) generated via interaction of an ascending hot plume with ambient air. Fire whirls are affected by local wind shear as well as the local topography. In addition to the capability of altering flame structure, wind can result in local areas of smoke removal with or without the occurrence of fire whirls. Such effects have been observed in fire whirls produced by JP4 and JP8 fuel fires in the presence of wind (Tieszen 1996). As shown in Figure 7 experiments with an 18.9 m JP-8 pool fire in a 2-4 m/s wind have demonstrated that fire whirls will occur at the downwind edge of the fire plume forming fire whirls, resulting in removal of smoke and allowing luminous zones to be exposed (Tieszen 1996). These tests indicate that the formation of these vortex structures occur at regular intervals and are roughly half a diameter in extent. They can occur in pairs or alternate from side to side. This affect will change the surface emissive power not only by the removal of smoke, but also due to the increased surface emissive power associated with fire whirls. Due to the high combustion rates in these vortices very high spot SEP values occur.

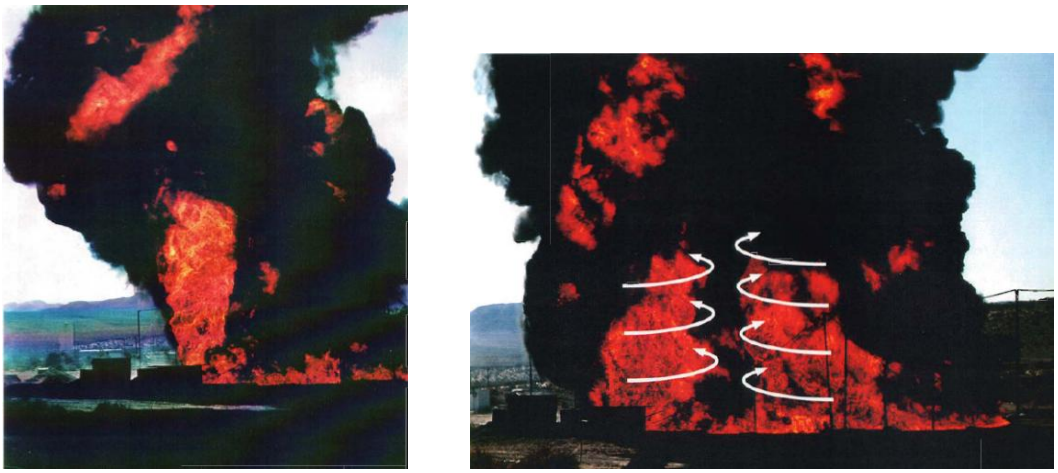

Figure 7: Fire whirls forming on the downwind edge of an 18.9 m JP-8 pool fire in a 2-4 m/s wind **(Tieszen 1996)**.

3.4 Water Conditions

During LNG test 2 (Blanchat, et al. 2011) a layer of methane hydrate formed encompassing the 56 meter diameter burning region. The effective diameter of the hydrate layer is approximately 83 meters. Methane hydrates are ice-like compounds where water molecules interstitially encage CH_4 gas molecules and is comprised of $CH_4 \cdot nH_2O$ ($n \geq 5.75$). Methane hydrates typically are found to occur in high-pressure low-temperature environments. They can however be found at 1 atmosphere under low temperatures near and below the freezing temperature of water, but they are not stable. This state is termed metastable and dissociation to H_2O ice + CH_4 gas at 0.1 MPa can be on the order of minutes to hours between the temperatures of 242 – 273 K (Stern 2001). Stern, et al. found that dissociation behavior is dependent on the pressure-temperature-time path taken to create a metastable state. Rapid depressurization of methane hydrate at isothermal conditions results in an anomalous region where the dissociation rate is non-monotonic with temperature and the stability is greater between 242 and 271 K than below 240 K, whereas slow-warming does not result in this anomalous behavior (Stern 2001). For equilibrium stability at atmospheric pressure methane gas hydrate must be at a temperature of 193 K or below. Mixtures of methane, ethane, and propane representative of natural gas does not show this anomalous behavior, though they have displayed stable behavior up to 256 hours at 1 atmosphere for the temperature range of 268.2 - 270.2 K when achieved through certain pressure-temperature paths (Zhang 2008). These studies demonstrate that there are methods to achieve metastable states at 1 atmosphere near water-freezing temperatures such as through rapid depressurization. The methods used are different than the dynamics of the SNL tests in that very cold liquid methane is being mixed with much higher temperature water. It can be anticipated that ice and/or hydrates will form particularly when the water temperature is near 273 K and even at warmer temperatures, though their stability will significantly decrease with warmer water and with surrounding agitation, such as, from the spill itself and/or ocean conditions.

Expectation are that the heat flux from the flame would melt the ice/hydrate layer or prevent its formation even in near water-freezing temperatures. In the 83-m test, burning was prevented due to the previously mentioned extinction mechanism and the presence of water vapor that attenuated the radiation from the flame to prevent melting. The level of attenuation was significant given that the flame ignited scrub grass near the south pool edge approximately 20 to 30 m away but could not melt the adjacent hydrate layer. The very cold hydrate layer provided a suitable environment for a thick layer of water vapor from the pool and environment to condense and form above it. The water vapor was continually transported across this layer due to entrainment. Evidence of hydrates is shown in Figure 8 which shows that near the end of the test the fire significantly decreased then spread, extending beyond the tip of the diffuser and subsequently burned in isolated regions across the pool area indicating the presence of fuel. With the occurrence of a smaller fire near the end of the test, the entrainment and the consequent protective water vapor layer above the pool decreased thereby allowing the warming of the hydrate and ignition of the released fuel.

Figure 8: Sequence of late-time burning of the hydrates during the 83-m SNL test resulting in a 56-m fire.

The amount of LNG encased in the hydrate for the 83-m test is uncertain but there are indications that it was mostly comprised of ice since the duration of late-time burning was relatively short and the burn area was very limited. Assuming a hydrate thickness of approximately 0.01 m and surface area of roughly 3,700 m^2 it can be estimated that about 10 m^3 (2640 gallons) of equivalent LNG was encased in the hydrate layer which is about 5% of the LNG spilled (see Appendix for derivation). This most likely is an upper bound estimate.

The formation of a hydrate layer also formed in the 21 m diameter SNL test, but not nearly of the same magnitude as shown in Figure 9. Beyond the amount spilled, the difference between the 21 m and 83-m tests is the temperature of the water where temperatures of 277 K and 274 K were measured, respectively. Since the water temperature was near freezing (274 K) for the 83- m test the propensity to form hydrates was enhanced. The amount of hydrate formation for the 21 m test was considerably less relative to the burning region than the 56 m test which is most likely due to the higher water temperature. Further indication of the effect of water temperature can be deduced from the 10 m SNL test. This test was performed on a pool 15.2 m deep with a temperature around 280 K and did not produce a significant amount of hydrates; rather small isolated pieces which quickly melted were evident post-test. These possibly could have been only ice and not hydrates. The 10 m test also had a vertically directed fuel release compared to the horizontal directed release of the large tests. A vertical fuel release will promote mixing with

the much warmer water. A test, possibly similar to the 10 m test, at water temperatures near freezing would allow for the effects of water temperature and spill rate to be isolated.

Figure 9: Post-test hydrate layer in the 21 m SNL test.

With regards to the locations of LNG ports, formation of hydrates may be an issue for certain locations that have water temperatures near freezing. However, in ocean environments the presence of salinity and waves will reduce the probability of formation (Tishchenko 2005). If a hydrate layer does form its effect will be to reduce the burning region to result in a smaller pool fire. Thus, a conservative assumption for ports in near-freezing locations is no hydrate formation.

4 RECOMMENDATIONS

The solid flame model requires knowledge of the burn rate, flame height, surface emissive power and transmissivity. Since it is very difficult to obtain measurements of flame emissivity and temperature a global value for SEP is instead obtained experimentally which can be used in solid flame models. The following provides recommendations on these parameter values based upon data obtained from the SNL tests which are the largest LNG pool fire tests performed on water or land to date.

4.1 Burn rate

The average burn rate based on SNL Test 1 is 0.147 ± 0.01 kg/m^{2}s or 3.5 x 10^{-4} m/s, dividing by the liquid density of 420 kg/m^3 (Blanchat, et al. 2011). The variation is over time. The reported uncertainty is ±20.4% which provides the range of 2.6 x 10^{-4} m/s to 4.5 x 10^{-4} m/s. The burn rate was not obtained from SNL Test 2 due to the lack of achieving a steady state between the inflow and pool diameter, as well as the presence of a hydrate layer. As noted previously wind will tend to increase the burn rate. Since SNL Test 1 was performed in a nominal wind condition of 4.5 m/s it can be estimated that the burn rate was increased by approximately 20%. A 20% lower burn rate is still within the range of uncertainty. Note that the dynamics of the pool is affected by waves, currents, wind, and the impact of the spill source. The interaction can be very complex and will affect the burn rate. This requires additional research and was not within the scope of any LNG test series to date.

The only other experiment able to derive burn rate data for LNG pool fires on water are the tests funded by the USCG which reported calculated burn rates ranging from $4x10^{-4}$ to $11x10^{-4}$ m/s. The calculations use the total quantity spilled divided by the approximate pool area and time of 'intense' burning to derive the burn rate. The volume spilled during steady state burning was less than the total volume of LNG spilled. By using the total volume of LNG spilled rather than the volume spilled during steady burning, higher burn rates are calculated. If burn rates are calculated based upon dividing the reported values for spill rate by the pool area, then burn rates vary from $2.6\ x10^{-4}$ to $9x10^{-4}$ m/s.

Since the burn rate is a function of the heat transfer from the flame and from the water, the range of burn rates for LNG pool fires on water can be estimated by combining data from pool fire experiments on land and un-ignited spill tests on water. The Montoir tests report an average mass burn rate of 0.14 kg/m^2 s performed in wind speeds that ranged from about 3 – 10 m/s. The mass burn rate was calculated from dip tube measurements assuming a liquid density of 500 kg/m^3. This indicates a burn rate of 2.8×10^{-4} m/s for an LNG pool fire on land. The range of burn rate values derived from *un-ignited* LNG pools on water range from 0.64×10^{-4} to 4.3×10^{-4} m/s (Luketa-Hanlin 2006). If these values are added to the Montoir data, the range of burn rate values for pool fires on water would be 3.4×10^{-4} to 7.1×10^{-4} m/s. Note that the USCG tests extend outside this region. The discrepancy between considering fires on water and reacting/non-reacting separately can be due to inadequate measurements, differences in LNG composition, and different wind conditions.

Based on the test results, the recommended average burn rate is 3.5×10^{-4} m/s and the recommended range is 2.6×10^{-4} m/s to 4.5×10^{-4} m/s for parametric variation analysis. Related to the burn rate is the formation of hydrates since both affect pool size. For port locations that have a potential for hydrate formation it is recommended that a conservative assumption is used for safety purposes, namely that no hydrate formation occurs.

4.2 Flame Height

Recommendation on flame height is based on data collected from reduced scale methane tests performed at the Thermal Test Complex at Sandia as shown in Figure 10.

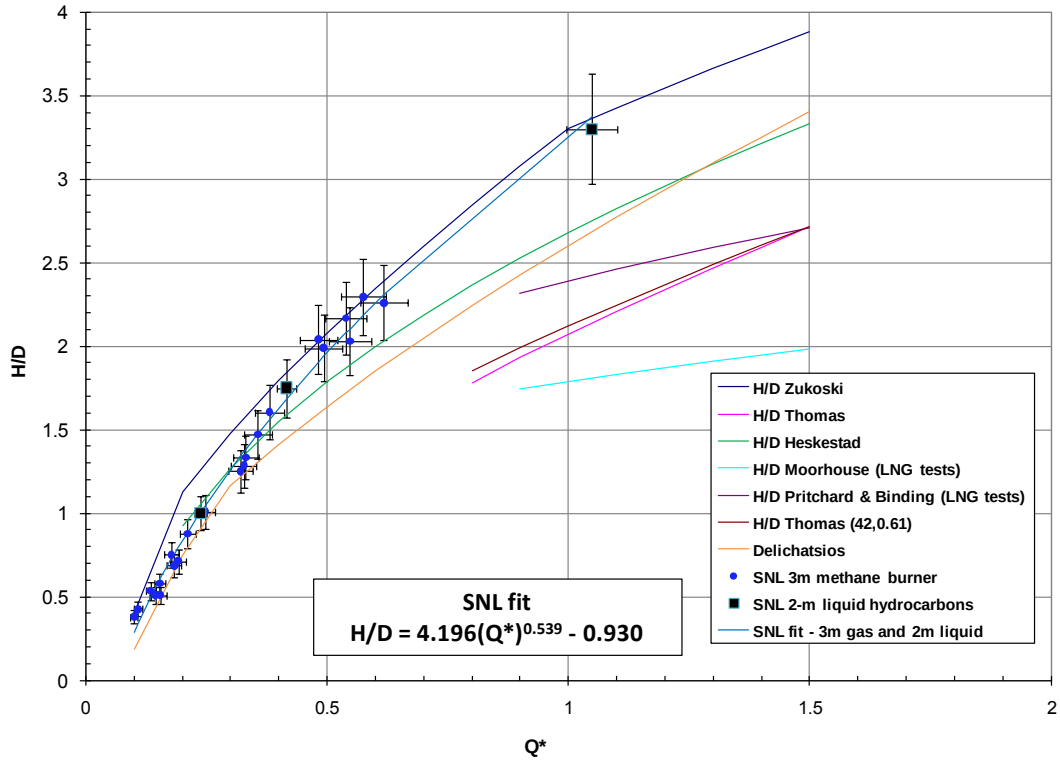

Figure 10: Flame height/diameter ratio vs. dimensionless heat release rate Q*.

The SNL data can be fit with the curve of

$$H/D = 4.196Q^{*0.539} - 0.930. \quad (1)$$

The uncertainty on the flow measurements is 8% (2 standard deviations) and the uncertainty on the flame height data is 10%. The combination of this uncertainty results in an uncertainty range that can be represented by high and low correlations of similar form to eq (1). They are the following.

$$H/D = 4.828Q^{*0.539} - 1.023. \quad \text{(high range of uncertainty)} \quad (1a)$$

$$H/D = 3.623Q^{*0.539} - 0.837. \quad \text{(low range of uncertainty)} \quad (1b)$$

It is recommended that eq. (1) with the uncertainty range represented through eqns. (1a) and (1b) be used to predict flame height, applicable for the Q* range of 0.1 to 1. For sites with appreciable wind, a conservative answer will be provided by using the SNL flame height correlation since it was obtained under quiescent conditions and wind tends to result in lower flame heights.

These tests acquired data on flame height for particular Q* values which is a dimensionless heat release rate parameter that has been found to correlate with flame height. Q^* is of the following form

$$Q^* = \frac{\dot{m}\Delta H}{\rho_a T_a C_{p_a} \sqrt{g} D^{5/2}} \qquad (2)$$

where $\dot{m}$ is the fuel mass loss rate in units of kg/s, ΔH is the heat of combustion (50 MJ/kg for methane), and the thermal properties, ρ_a, C_{pa}, and T_a are evaluated at surrounding conditions. Q* values can be evaluated by using eq. (2) and a corresponding burn rate, diameter, and appropriate atmospheric conditions. The H/D value for a calculated Q* value can then be determined using eq. (1). Several other correlations obtained with smaller burners (up to 0.5 m diameter) are also shown in Figure 10 and indicate agreement with the SNL flame height correlation which utilized the largest burner to date of 3-m in diameter. The Thomas (Thomas 1963), Moorhouse (Moorhouse 1982), and Pritchard (Pritchard and Binding 1984) correlations are plotted over a Q* range for which they were derived. The extrapolation of the Moorhouse and Thomas correlations to lower Q* values will be discussed in a following section.

For reference, Table 2 shows that a Q* range of approximately 0.1 to 1 corresponds to a diameter range of about 25 m to 2200 m. The Q* values calculated in Table 2 are based upon the standard atmospheric properties of T_a=300 K, ρ_a=1.17 kg/m^3, and C_{pa}=1006 J/kg K. The product of $\rho_a T_a C_{pa}$ does not change appreciably for constant pressure regardless of temperature since C_{pa} is fairly constant over typical temperature ranges and $\rho_a T_a$ remains constant through the ideal gas law. However, for high altitude conditions the pressure will be lower than sea level conditions and Table 2 is not applicable. The nominal burn rate of 0.147 kg/m^2 s was also used and must be multiplied by the pool area to provide units of kg/s for use in eq. (2).

Table 2: H/D ratio for various diameters and corresponding Q* values based on SNL flame height correlation.

Diameter (m)	Q*	H/D (SNL)
25	1.046	3.369
50	0.740	2.637
75	0.604	2.268
100	0.523	2.029
200	0.370	1.525
300	0.302	1.271
400	0.262	1.107
500	0.234	0.988
600	0.214	0.896
700	0.198	0.822
800	0.185	0.760
900	0.174	0.708
1000	0.165	0.662
1100	0.158	0.621
1200	0.151	0.585
1300	0.145	0.553
1400	0.140	0.524
1500	0.135	0.497
1600	0.131	0.472
1700	0.127	0.450
1800	0.123	0.429
1900	0.120	0.409
2000	0.117	0.391
2100	0.114	0.373
2200	0.112	0.357

4.3 Surface Emissive Power

For SNL Test 1 and 2, the surface emissive power (SEP) derived from wide-angle radiometer measurements and actual flame shape based on video analysis are 277 ±60 kW/m^2 and 286 ±20 kW/m^2, respectively. The variation is based upon differences of time-averaged values among the radiometers. The reported uncertainty is ±10%. It is recommended that the SEP value from SNL Test 2 is applied since it is the largest test. One of the main questions to be addressed from the experiments was the occurrence of smoke shielding as a function of scale. As previously discussed, Test 2 did not exhibit significant smoke shielding. Thus, based on these findings it is

recommended that the SEP value of 286 ±20 kW/m^2 be applied without adjustment for smoke shielding. However, for very large fires some smoke shielding most likely will be present, but in consideration of the potential effect of water on smoke production through suppressed soot production and enhanced soot oxidation, as well as the effects of wind concerning smoke-shedding and counter-rotating vortices as previously discussed this recommendation is warranted for safety purposes. Thus, the recommended average SEP is 286 kW/m^2 and the recommended range for parametric variation is 239 kW/m^2 to 337 kW/m^2.

4.4 Atmospheric Attenuation (transmissivity)

The attenuation of radiation by absorption and scattering through the atmosphere was calculated using surrounding atmospheric properties for both Sandia large scale LNG fire tests (Blanchat, et al. 2011) and transmissivity as a function of distance was obtained. The level of uncertainty is estimated to be ±10%. The transmissivity will decrease with increasing levels of relative humidity and atmospheric temperature, thus it is desirable to have an equation that incorporates these factors. The SNL data does not cover a wide range of relative humidity levels and atmospheric temperatures, but comparison with a formula developed by Wayne (Wayne 1991) indicates very close agreement to the SNL data as shown in Figure 11. The formula assumes a black or grey body source with a temperature of 1500 K and is applicable over the atmospheric temperature range of 253 – 313 K. The equation is of the following form.

$$\tau = 1.006 - 0.01171\log_{10} X(H_2O) - 0.02368(\log_{10} X(H_2O))^2 - 0.03188\log_{10} X(CO_2) + 0.001164(\log_{10} X(CO_2))^2 \quad (3)$$

with,

$$X(H_2O) = (R_H L P\ 2.8865x10^2)/T$$

$$X(CO_2) = 273L/T$$

$X(H_2O)$ and $X(CO_2)$ are the amount of H_20 and CO_2 along a path length, L (m). R_H is the relative humidity (0 – 1.0) and S is the saturated water vapor pressure in mm of mercury at the atmospheric temperature T (K). The saturated water vapor pressure can be determined from the Antoine formula where the coefficients are from Stull (Stull 1947) applicable over the temperature range 255.8 – 373 K.

$$\log_{10} P = 4.65430 - \frac{1435.264}{T - 64.848} \quad (4)$$

The pressure, P, must be converted from bar to mm mercury by multiplying eq. (4) by 750.061. Since eq. (3) encompasses a wide range of relative humidity levels and atmospheric temperatures as well as having very close agreement with the SNL data it is recommended that eq. (3) is used to calculate transmissivity. To illustrate the effect of atmospheric temperature and relative

humidity Figure 12 shows the difference in transmissivity between two extreme temperature and relative humidity conditions. The temperature and relative humidity condition of 269 K (25^{o}F) and 10% provides transmissivity values that are from 20% to 60% higher along the path length compared to a condition with a temperature of 310 K(98^{o}F) and 100% relative humidity. Thus, the lower temperature and relative humidity condition would result in a higher thermal hazard distance.

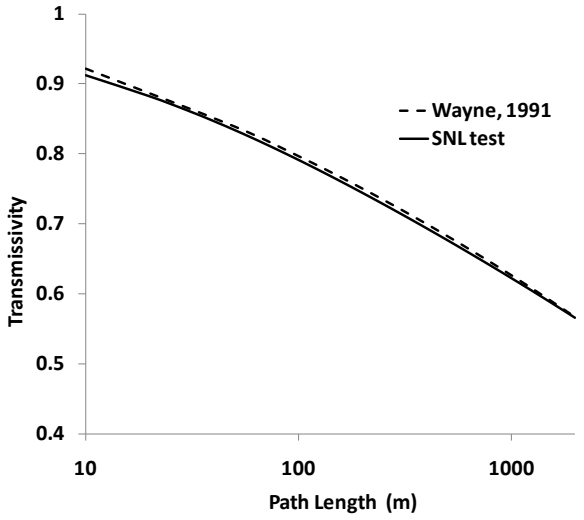

Figure 11: Comparison of transmissivity over path length between SNL data and formula by Wayne, 1991.

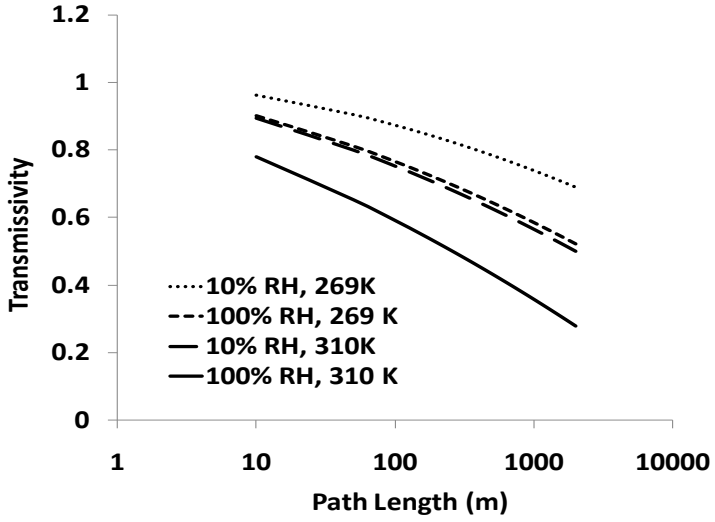

Figure 12: Effect of relative humidity and temperature variation on transmissivity.

5 COMPARISON TO 2004 AND 2008 SANDIA LNG REPORTS

The recommended parameter values in the 2004 and 2008 Sandia LNG reports (Hightower 2004) (Luketa 2008) were based on knowledge of test data available at the time. In this report, the recommended values have been updated based on the recent data collected from the Sandia large scale LNG tests as discussed in section 4. Table 3 provides a comparison between the previous and current recommendations for reference.

Table 3: Comparison of recommended parameter values for solid flame model.

Nominal value	***2004 and 2008 Sandia LNG reports***	***Current report***
Burn rate (m/s)	3.0×10^{-4}	3.5×10^{-4}
Flame height (m)	Moorhouse correlation	SNL correlation, eq. (1) (reduced scale data)
SEP (kW/m^2)	220	286
Transmissivity	0.8	Wayne formula, eq. (3) (compared with SNL data)

Table 4 provides predicted thermal hazard distances for intentional events using the updated parameters and the same scenario matrix for hole size and tanks breached as the 2004 report, shown in Table 5. The average pool size is calculated using the same approach as in the 2004 report and the discharge coefficients also have not changed. Note that the calculated pool diameter for the nominal case in Table 4 is representative of pool diameters calculated using CFD in the recent analysis of (Figueroa and Lopez, 2011) where for nominal large spills the pool diameters ranged from 330 m to 350 m. Variation of the parameters in Table 4 is based on reported uncertainty values from the test data. A relative humidity of 20% and surrounding temperature of 269 K (25^oF) was used in the transmissivity function as a nominal case. These values were used in order to have a fair comparison to the constant transmissivity value of 0.8 used in the 2004 report which is more reflective of low temperature and relative humidity conditions. The low transmissivity variation was calculated using a relative humidity of 100% and temperature of 310 K. The updated parameter values result in an average thermal hazard distance of about 1275 m to the 5 kW/m^2 heat flux level or about a 2% decrease in the thermal hazard distance of 1305 m predicted in the 2004 report. For locations with high humidity and temperatures year around this distance can potentially decrease between 20-30% due to decreased transmissivity levels. It is important to realize that the scenario matrix in Table 4 does not apply to all sites. As stressed in the 2004 Sandia report, site-specific hazard analyses should be performed that incorporates surrounding conditions and appropriate scenarios. Thus, the distances provided in Table 4 will change depending on the site.

Comparison to the 2008 Sandia report (Luketa 2008) for large LNG carriers (~250,000 m^3 class) using the updated parameters is provided in Tables 6 – 9 for both near-shore and off-shore operations. For near-shore operations using the updated parameters the thermal hazard distance to the 5 kW/m^2 level results in approximately a 7% reduction from 1383 m to 1289 m. For off-shore operations using the updated parameters the thermal hazard distance to the 5 kW/m^2 level also results in approximately an 8% reduction from 2030 m to 1872 m.

Table 4: Thermal hazard distances using recommended parameter values based on SNL test data.

HOLE SIZE (m^2)	TANKS BREACHED	DISCHARGE COEFFICIENT	BURN RATE (m/s)	SURFACE EMISSIVE POWER (kW/m^2)	τ	POOL DIAMETER (m)	BURN TIME (min)	DISTANCE TO	
								37.5 kW/m^2 (m)	5 kW/m^2 (m)
INTENTIONAL EVENTS									
2	3	0.6	3.5×10^{-4}	286	nom	194	20	295	893
5	3	0.6	3.5×10^{-4}	286	nom	530	8.1	690	1902
5*	1	0.6	3.5×10^{-4}	286	nom	306	8.1	436	1266
5	1	0.3	3.5×10^{-4}	286	nom	216	16	324	973
5	1	0.6	2.6×10^{-4}	286	nom	355	8.1	461	1248
5	1	0.6	4.5×10^{-4}	286	nom	270	8.1	408	1261
5	1	0.6	3.5×10^{-4}	286	low	306	8.1	320	922
5	1	0.6	3.5×10^{-4}	239	nom	306	8.1	388	1162
5	1	0.6	3.5×10^{-4}	337	nom	306	8.1	483	1370
12	1	0.6	3.5×10^{-4}	286	nom	474	3.4	629	1755

*nominal case

Table 5: Thermal hazard distances predicted in the 2004 Sandia Report **(Hightower 2004)**.

HOLE SIZE (m^2)	TANKS BREACHED	DISCHARGE COEFFICIENT	BURN RATE (m/s)	SURFACE EMISSIVE POWER (kW/m^2)	τ	POOL DIAMETER (m)	BURN TIME (min)	DISTANCE TO	
								37.5 kW/m^2 (m)	5 kW/m^2 (m)
INTENTIONAL EVENTS									
2	3	.6	3×10^{-4}	220	.8	209	20	250	784
5	3	.6	3×10^{-4}	220	.8	572	8.1	630	2118
5*	1	.6	3×10^{-4}	220	.8	330	8.1	391	1305
5	1	.3	3×10^{-4}	220	.8	233	16	263	911
5	1	.6	2×10^{-4}	220	.8	395	8.1	454	1438
5	1	.6	8×10^{-4}	220	.8	202	8.1	253	810
5	1	.6	3×10^{-4}	220	.5	330	8.1	297	958
5	1	.6	3×10^{-4}	175	.8	330	8.1	314	1156
5	1	.6	3×10^{-4}	350	.8	330	8.1	529	1652
12	1	.6	3×10^{-4}	220	.8	512	3.4	602	1920

*nominal case

Table 6: Thermal hazard distances for large LNG carriers operating in near-shore conditions using recommended parameter values based on SNL test data.

HOLE SIZE (m^2)	TANKS BREACHED	DISCHARGE COEFFICIENT	BURN RATE (m/s)	SURFACE EMISSIVE POWER (kW/m^2)	τ	POOL DIAMETER (m)	BURN TIME (min)	DISTANCE TO	
								37.5 kW/m^2 (m)	5 kW/m^2 (m)
INTENTIONAL EVENTS									
2	3	0.6	3.5×10^{-4}	286	nom	208	57	313	944
5	3	0.6	3.5×10^{-4}	286	nom	569	23	732	2005
5*	1	0.6	3.5×10^{-4}	286	nom	329	23	463	1338
5	1	0.3	3.5×10^{-4}	286	nom	232	46	345	1029
5	1	0.6	2.6×10^{-4}	286	nom	381	23	489	1314
5	1	0.6	4.5×10^{-4}	286	nom	290	23	434	1333
5	1	0.6	3.5×10^{-4}	286	low	329	23	333	969
5	1	0.6	3.5×10^{-4}	239	nom	329	23	413	1227
5	1	0.6	3.5×10^{-4}	337	nom	329	23	513	1446
12	1	0.6	3.5×10^{-4}	286	nom	509	10	668	1849

Table 7 Thermal hazard distances for large LNG carriers operating in near-shore conditions predicted in the 2008 Sandia Report for large LNG carriers (Luketa 2008).

HOLE SIZE (m^2)	TANKS BREACHED	DISCHARGE COEFFICIENT	BURN RATE (m/s)	SURFACE EMISSIVE POWER (kW/m^2)	τ	POOL DIAMETER (m)	BURN TIME (min)	DISTANCE TO	
								37.5 kW/m^2 (m)	5 kW/m^2 (m)
INTENTIONAL EVENTS									
2	3	0.6	3×10^{-4}	220	0.8	225	57	282	881
5	3	0.6	3×10^{-4}	220	0.8	615	23	774	2197
5*	1	0.6	3×10^{-4}	220	0.8	355	23	446	1344
5	1	0.3	3×10^{-4}	220	0.8	251	46	315	975
5	1	0.6	2×10^{-4}	220	0.8	435	23	547	1487
5	1	0.6	8×10^{-4}	220	0.8	217	23	273	1042
5	1	0.6	3×10^{-4}	220	0.5	355	23	305	1050
5	1	0.6	3×10^{-4}	175	0.8	355	23	373	1188
5	1	0.6	3×10^{-4}	350	0.8	355	23	617	1683
12	1	0.6	3×10^{-4}	220	0.8	550	10	692	1981

Table 8: Thermal hazard distances for large LNG carriers operating in off-shore conditions using recommended parameter values based on SNL test data.

HOLE SIZE (m^2)	TANKS BREACHED	DISCHARGE COEFFICIENT	BURN RATE (m/s)	SURFACE EMISSIVE POWER (kW/m^2)	τ	POOL DIAMETER (m)	BURN TIME (min)	DISTANCE TO	
								37.5 kW/m^2 (m)	5 kW/m^2 (m)
INTENTIONAL EVENTS									
5	3	0.6	3.5×10^{-4}	286	nom	569	23	732	2005
12	3	0.6	3.5×10^{-4}	286	nom	882	9.6	1043	2732
12*	1	0.6	3.5×10^{-4}	286	nom	509	9.6	668	1849
12	1	0.3	3.5×10^{-4}	286	nom	360	19	500	1432
12	1	0.6	2.6×10^{-4}	286	nom	591	9.6	693	1782
12	1	0.6	4.5×10^{-4}	286	nom	449	9.6	632	1862
12	1	0.6	3.5×10^{-4}	286	low	509	9.6	473	1309
12	1	0.6	3.5×10^{-4}	239	nom	509	9.6	599	1700
12	1	0.6	3.5×10^{-4}	337	nom	509	9.6	734	1996
16	1	0.6	3.5×10^{-4}	286	nom	588	7.2	752	2052

Table 9: Thermal hazard distances for large LNG carriers operating in off-shore conditions predicted in the 2008 Sandia Report for large LNG carriers (Luketa 2008).

HOLE SIZE (m^2)	TANKS BREACHED	DISCHARGE COEFFICIENT	BURN RATE (m/s)	SURFACE EMISSIVE POWER (kW/m^2)	τ	POOL DIAMETER (m)	BURN TIME (min)	DISTANCE TO	
								37.5 kW/m^2 (m)	5 kW/m^2 (m)
INTENTIONAL EVENTS									
5	3	0.6	3×10^{-4}	220	0.8	615	23	774	2196
12	3	0.6	3×10^{-4}	220	0.8	953	9.6	1090	3168
12*	1	0.6	3×10^{-4}	220	0.8	550	9.6	692	1980
12	1	0.3	3×10^{-4}	220	0.8	389	19	466	1429
12	1	0.6	2×10^{-4}	220	0.8	674	9.6	786	2335
12	1	0.6	8×10^{-4}	220	0.8	337	9.6	407	1261
12	1	0.6	3×10^{-4}	220	0.5	550	9.6	462	1539
12	1	0.6	3×10^{-4}	175	0.8	550	9.6	553	1738
12	1	0.6	3×10^{-4}	350	0.8	550	9.6	864	2452
16	1	0.6	3×10^{-4}	220	0.8	635	7.2	741	2202

It is of interest to determine how the recommended nominal values in the 2004 and 2008 Sandia reports and the current recommendations compare to measured heat flux values from the SNL LNG Test 2 (Blanchat, et al. 2011) . Table 10 shows the predicted and measured heat flux values

from the 83- m diameter SNL LNG Test 2 using the models and nominal parameters used in the 2004 and 2008 Sandia reports and the current recommendations. Note that in column 2 of Table 10 the plus/minus variation in experimental values is one standard deviation over the time averaging interval from 250 to 300 seconds. The value in parentheses in column 2 is the upper bound determined from adding the standard deviation to the average value and increasing by the reported experimental uncertainty of 10%. The distances at which the comparisons were made were shifted 23 m determined from the experiment (Blanchat, et al. 2011) to account for the location of the fire that is anchored downwind of the release point. Thus, 23 m was subtracted from the South spoke distances and 23 m added to the North spoke distances.

The comparison indicates that the predicted heat flux values using the recommended nominal parameters from the 2004/2008 reports are slightly below experimental heat flux values that include uncertainty. The current recommended parameters provide heat flux values higher than the average experimental values. Representing the flame as a cylinder over-predicts the view factor as compared to that from the actual flame shape. Hence the predicted heat flux values at the various distances are expected to be higher than experimental average values. For this pool diameter, the parameter values used in the 2004/2008 reports are slightly under predictive. However, for larger pool diameters the 2004/2008 reports provide slightly higher hazard distances than current recommended parameter values. This is mainly due to differences in the flame height correlations and transmissivity values.

Table 10: Comparison of former and current parameter recommendation to SNL test 2.

Distance (m)	***Heat flux (kW/m^2)***		
South spoke	Experiment* Upper bound in parentheses	2004/2008 Sandia report prediction	Current report prediction
87	31.5 ± 2.7 (37.6)	29.0	43.5
137	16.1 ± 1.4 (19.3)	14.4	23.2
187	9.9 ± 0.9 (11.9)	8.3	14.1
North Spoke			
133	16.5 ± 1.2 (19.5)	15.1	24.3
183	9.7 ± 0.7 (11.4)	8.6	14.6
233	6.4 ± 0.4 (7.5)	5.5	9.6

*experimental uncertainty is ±10%.

To explain the impact of flame height prediction on the behavior of this difference, Figure 13 provides a comparison among the SNL, Moorhouse (Moorhouse 1982), and Thomas (Thomas 1963) correlations. The Thomas correlation was not used in the 2004 Sandia report, but is compared here since it is a widely used correlation. The Moorhouse correlation is in fairly close agreement with the SNL correlation for diameters between 200 and 400 m, but predicts a higher flame height than the SNL correlation for diameters above 300 m, while the Thomas correlation predicts a lower flame height than the SNL and Moorhouse correlations for diameters up to

about 1500 m. Thus, the SNL flame height correlation will provide lower thermal hazard distance than the Moorhouse correlation for pool diameters above 300 m and is partially responsible for the lower thermal hazard distances provides in Table 4. The difference in transmissivity is also responsible where the current recommend function, eq. (3), provides decreasing transmissivity values as a function of distance, while a constant value of 0.8 was used in the 2004/2008 Sandia reports. The slightly higher recommended burn rate provides some reduction as well but not to a great extent. However, the effect of these three parameters in reducing thermal hazard distances is offset by the increased average surface emissive power of 286 kW/m^2 versus 220 kW/m^2.

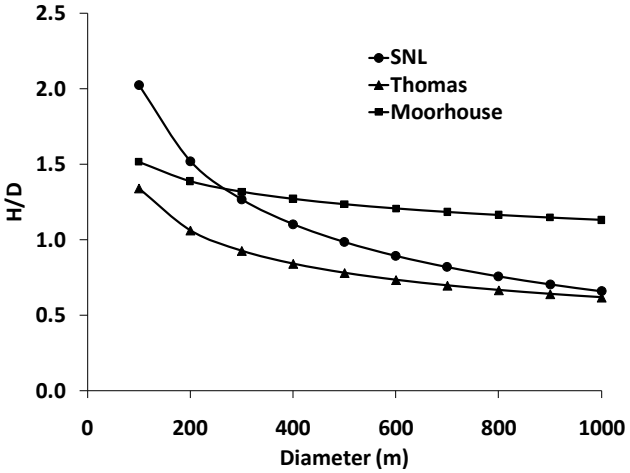

Figure 13: Comparison of SNL, Moorhouse, and Thomas flame height correlations.

6 SUMMARY

This report has provided discussion of the various factors that affect the dynamics of LNG pool fires, as well as the parameters required for the solid flame model for hazard prediction. Recommendations on parameter values for solid flame models, shown in Table 11, have been provided based on large scale LNG pool fire tests conducted at Sandia (Blanchat, et al. 2011). The updated recommendations are considered conservative and result in approximately 2% and 7-8% lower thermal hazard distances than provided in the 2004 and 2008 Sandia reports, respectively (Hightower, et al. 2004, Luketa, et al. 2008). Additional physics that occurred during the LNG pool fire tests have been discussed such as hydrate formation and flame stability. Since it is very difficult to predict the extent of non-burning regions across the pool it is recommended for safety purposes to assume the pool area is fully burning. It must be emphasized as in the 2004/2008 Sandia reports that hazard distances will change depending on the surroundings conditions and the scenarios associated with the site. Thus, site-specific analyses should be performed.

Table 11: Recommended parameter values for solid flame model.

Parameter	***Recommended nominal value***
Burn rate (m/s)	3.5×10^{-4} $(2.6 – 4.5 \times 10^{-4})$*
flame height (m)	SNL correlation, Eq. (1) (eqns. 1a, 1b)*
SEP (kW/m^2)	286 (239 – 337)*
Transmissivity	Wayne formula, Eq. (3) (±10%)

*range of uncertainty

REFERENCES

Atreya, A., Crompton, T., Suh, J. "A Study of the Chemical and Physical Mechanisms of Fire Suppression by Water." *Fire Safety Science: Proceedings of the Sixth Int. Sym.* 1999. 493-504.

Blanchat, T. K., Manning, L. "Mock B52 Bomb Bay Fire Experiment Data and Analysis for Model Validation and Development." SAND2002-0145, 2002.

Blanchat, T. K., Sundberg, D., Brown, A. "Well-characterized Open Pool Experiment Data and Analysis for Model Validation and Development." SAND2006-7508, 2006.

Blanchat, T., P. Helmick, R. Jensen, A. Luketa, and R., Suo-Anttila, J., Mercier, J., Miller, T., Ricks, A., Simpson, R., Demosthenous, B., Tieszen, S., and Hightower, M. Deola. "The Pheonix Series Large Scale LNG Pool Fire Experiments." SAND2010-8676 , 2011.

British Gas. "Results of detailed measurements made on a 35m diameters LNG pool fire experiment conducted at Montoir." 3 volumes, 1988.

Castineira, D., Edgar, T. F. "CFD for Simulations of Steam-Assisted and Air-Assisted Flare Combustion Systems." *Energy and Fuels*, 2006: 1044-1056.

Corlett, R.C., Luketa-Hanlin, A. "Pressure Scaling of Fire Dynamics." In *Progress in Scale Modeling*, edited by Z. Saito, 85-97. Springer, 2008.

Dryer, F. L. "Water Addition to Practical Combustion Systems - Concepts and Applications." *Symposium (International) on Combustion* 16 (1977): 279-295.

Hightower, M., Gritzo, L., Luketa-Hanlin, A., Covan, J., Tieszen, S., Wellman, G., Irwin, M., Kaneshige, M., Melof, B., Morrow, C., Ragland, D. "Guidance on Risk Analysis and Safety Implications of a Large Liquefied Natural Gas (LNG) Spill Over Water." SAND2004-6258, 2004.

Luketa, A., Hightower, M., Attaway, S. "Breach and Safety Analysis of Spills Over Water from Large Liquefied Natural Gas Carriers." SAND2008-3153, 2008.

Luketa-Hanlin, A. "A review of large-scale LNG spills: experiments and modeling." *J. Hazardous Materials* A132 (2006): 199-140.

McCrain, L.L. and Roberts, W.L. "Measurments of the Soot Volume Field in Laminar Diffusion Flames at Elevated Pressures." *Combustion and Flame* 140 (2005): 60-69.

Moorhouse, J. "Scaling criteria for pool fires derived from large scale experiments." *I. Chem.E. Symposium Series*, 1982: 165-179.

Mudan, Krishna S. "Thermal Radiation Hazards from Hydrocarbon Pool Fires." *Prog. Energy Combust. Sci.*, 1984: 59-80.

Mudan, Krisna S. "Geometric View Factors for Thermal Radiation Hazard Assessment." *Fire Safety Journal*, 1987: 89-96.

Muller-Dethlefs, K., Schlader, A.F. "The Effect of Stam on Flame Temperature, Burning Velocity and Carbon Formation in Hydrocarbon Flames." *Comustion and Flame*, 1976: 205-215.

Nedelka, D., et al. "The Montoir 35 m diameter LNG pool fire experiments." *Int. Conf. Liq. Nat. Gas.* 1989.

Pritchard, M.J., and T.M. Binding. "FIRE2: A new approach for predicting thermal radiation levels for hydrocarbon pool fires." *Sym. major hazards onshore and offshore*, 1984: 491-505.

Quintiere, J.G. "Scaling Applications in Fire Research." *Fire Safety Journal*, 1989: 3-29.

Raj, P.K. "Experiments involving pool and vapor fires from spills of liquefied natural gas on water." Arthur D. Little, 1979.

Rao, V.K., Bardon, M.F. "The Effect of Water on Gas Phase Soot Formation in Laminar Diffusion Flames." *Combustion and Flame*, 1984: 73-78.
Richard, J., Garo, J.P., Souil, J.M., Vantelon, J.P., Knorre, V.G. "Chemical and Physical Effects of Water Vapor Addition on Diffusion Flames." *Fire Safety Journal*, 2003: 569-587.
Smyth, K., Tjossem, P.J.H, Hamins, A., Houston Miller, J. "Concentration Measurements of OH and Equilibrium Analysis in a Laminar Methane-Air Diffusion Flame." *Combustion and Flame*, 1990: 366-380.
Soma, S., Saito, K. "Reconstruction of Fire Whirls Using Scale Models." *Combustion and Flame*, 1991: 269-284.
Stern, L.A., et al. "Anomolous Preservation of Pure Methane Hydrate at 1 atm." *Journal of Physical Chemistry B*, 2001: 1756-1762.
Stull, D.R. "Vapor Pressure of Pure Substances Organic Compounds." *Ind. Eng. Chem.*, 1947: 517-540.
Thomas, P.H. "The size of flames from natural fires." *9th Int. Combustion Symposium*, 1963: 844-859.
Tieszen, S.R., Nicolette, V.F., Gritzo, L.A., Holen, J.A., Murray, D., and Moya, J.L. *Vortical Structures in Pool Fires: Observation, Speculation, and Simulation.* SAND96-2607, Sandia National Laboratories, 1996.
Tishchenko, P., Hensen,T.C., Wallmann, K., Wong, C.S. "Calculation of the stability and solubility of methane hydrate in seawater." *Chemical Geology*, 2005: 37-52.
Tucker, R.F. "35 m LNG pool fire tests at Montoir 1987." 3 volumes, Thornton Research Center, 1988.
Wayne, D.F. "An Economical Foruma for Calculating Atmospheric Infrared Transmissivities." *J. Loss Prev. Process Ind.*, 1991: 85-92.
Zhang, C., Atreya, A., Lee, K. "Sooting Structure of Methane Counterflow Diffusion Flames with Preheated Reactants and Dilution by Products of Combustion." *Twenty-Fourth Symposium (Int.) on Comb.*, 1992: 1049-1057.
Zhang, G., Rogers, R. "Ultra-stability of Gas Hydrates at 1 atm and 268.2 K." *Chemical Engineering Science*, 2008: 2066-2074.
Zhao, D., Yamashita, H., Kitagawa, K., Aria, N., Furuhata, T. "Behavior and Effect on NOx Formation of OH Radical in Methane-Air Diffusion Flame with Steam Addition." *Combustion and Flame*, 2002: 352-360.

APPENDIX

A.1.Derivation of the amount of LNG encased in hydrate layer for 56 m diameter SNL LNG test.

Table A1 provides property values used in the derivation of the amount of LNG encased in the hydrate layer for the 56 m test.

Table A1: Property Values used in derivation

Property	*Value*
LNG density (111 K)	422 kg/m^3
Hydrate density	913 kg/m^3
Hydrate Molecular Weight	17.74 kg/kmol
LNG molecular weight	16 kg/kmol
Hydrate Formula	$CH_4 + 6H_2O$
Mole Fraction of CH_4	14.3 kmol%

First determine how many kmoles of CH_4 are in 1 m^3 of hydrate.

$$\frac{\left(913\,\frac{kg}{m^3}\right)\left(0.143\ \frac{kmol\ CH_4}{kmol\ hydrate}\right)}{\left(17.74\,\frac{kg}{kmol}\right)} = 7.36\ \frac{kmol\ CH_4}{m^3\ hydrate}$$

For methane liquid there is (422 kg/m^3)/(16 kg/kmol) = 26.38 kmol CH_4/m^3 LNG.

Thus,

$$\frac{7.36\ \frac{kmol\ CH_4}{m^3\ hydrate}}{26.38\ \frac{kmol\ CH_4}{m^3\ LNG}} = 0.28\,\frac{m^3 LNG}{m^3 hydrate}$$

The radius of the hydrate layer was approximately 40.5 m and the radius of the burning region was about 25 m. Thus, the area of the hydrate layer is roughly 3,700 m^2 for a circular configuration. This is an upper bound since the hydrate layer was not continuous and the portion on the leeward side of the flame was very scarce. It is difficult to determine the thickness of the layer but a rough estimate is 0.01 m. Thus, the volume of the hydrate layer is estimated to be 37 m^3 which means using the relation above that there was equivalently about 10 m^3 (2640 gallons) of LNG encased.

DISTRIBUTION

EXTERNAL DISTRIBUTION

1 Christopher J. Freitas
Program Manager, Natural Gas Storage, Pipeline Reliability, and LNG
Office of Oil and Natural Gas, FE-32
United States Department of Energy
PA-20/Forrestal Building
1000 Independence Ave., SW.
Washington, DC 20585

1 Bob Corbin
Director, Oil and Gas Global Security and Supply
Office of Oil and Natural Gas, FE-34
United States Department of Energy
PA-20/Forrestal Building
1000 Independence Ave., SW.
Washington, DC 20585

SANDIA INTERNAL DISTRIBUTION

1	MS0384	D. B. Dimos, 1500
1	MS0735	J. Merson, 6730
1	MS1104	M. Tatro, 6200
1	MS1108	M. M. Hightower, 6111
1	MS1135	R. D. Watkins, 1532
1	MS1135	T. K. Blanchat, 1532
1	MS1135	A. Luketa, 1532
1	MS1139	D. L. Miller, 1530
1	MS0899	RIM-Reports Management, 9532 (electronic copy)

Sandia National Laboratories